Final Report

Project Title: "A Bayesian Approach to Surface X-ray Diffraction: A Combined Experimental and Theoretical Methodology"

PI: Paul F. Lyman
Co-PI: Dilano K. Saldin

For period 9/15/2001 to 9/14/2005

Recipient: Board of Regents of the University of Wisconsin System, representing the University of Wisconsin-Milwaukee, PO Box 413, Milwaukee, WI 53201

DOE Award Number: DE-FG02-01ER45926

Anticipated unexpended funds : $0

Technical Report

Significant progress was made on the objectives of DOE Award during its tenure. Broadly, we describe these advances in terms of developments in the theoretical methods of data analysis (Sec. A) and experimental solutions of surface structures (Sec. B). To briefly reiterate, the goal of the research program is to develop and refine a new theoretical method, conceived by Prof. Dilano Saldin, of analyzing the intensity of x-rays diffracted from the surface of a solid, and to apply this method to experimental x-ray scattering data. We have termed this method PARADIGM, which stands for Phase and Amplitude Recovery And Diffraction Image Generation Method. Significant advances in the PARADIGM theory were made during the grant period, and experimental milestones have also been achieved. The two components of the research program worked in concert, each spurring progress in the other.

The analytical technique that Saldin's group developed provides a way of assigning phases to scattering amplitudes directly, without reference to any guessed or otherwise preconceived physical models. The algorithm is iterative, and alternately places constraints on the data in real space and reciprocal space. Eventually, the algorithm converges on a self-consistent, and most likely, assignment of phases, and thereby directly provides a model-independent structure. Such a direct method is important because conventional structural refinement methods rely on having a guess of the starting structure that sufficiently good that it may be refined into a model with the correct atomic positions. If the starting model has, for example, the wrong number or identity of atoms in the surface unit cell, it can never refine to the correct model. Even in cases where the starting model contains the correct number and identity of atoms, it is relatively easy for refinement routines to get trapped in false minima; finding a global minimum of a multi-parameter phase space is a notoriously difficult problem. The utility of the present method, then, stems from its ability to, independently of preconceived notions, identify robust starting models for testing by conventional refinement techniques.

During the grant period, significant progress was made on refining and extending this theory in two directions. On one hand, we were able to optimize the routines to handle the vagaries of real scattering data. As described briefly below, this effort has allowed the case of a surface with (symmetry-related) domains to be handled. In another vein, Saldin and coworkers have applied these ideas to the strong multiple-scattering case of low energy electron diffraction (LEED) with gratifying success.

A. Theoretical Developments

In this section, we give a rationale for, and an overview of, the theoretical method we have developed during the term of DOE support. This algorithm has allowed us to robustly recover the electron density in the near-surface region of several samples studied. First we present the general theoretical notions in Sec. A.1, and give some

particular details in Sec. A.2. Note that Sec. A.2.a gives the essential theoretical background necessary to understand our approach.

1. Historical Overview

There were a number of direct methods that had been suggested and applied to SXRD data before we began our work. We describe them briefly to provide a context for the method we have developed.

Yacoby and coworkers [1, 2] had developed a method, known by the acronym COBRA (standing for COherent Bragg Rod Analysis), which to date has been applied only to determine the structures of epitaxially grown atomic layers embedded in layers of a known structure. The method is applied solely to data of the crystal truncation rods (CTRs), which contain scattered-intensity contributions from the known parts of the structure, as well from unknown parts. If the structure under investigation has a larger 2D unit cell than that of the bulk, the method is capable of recovering only the so-called *folded* structure in which periodicities on a length scale larger than that of a bulk unit cell are folded back into a bulk unit cell.

Rius *et al*. [3] had proposed a method of phasing the "in-plane" superstructure Bragg spots to recover what is known as the *difference structure*, namely the difference between the true surface structure and the *folded* structure. As shown by Torrelles and co-workers [4, 5], for large surface unit cells this may be sufficient to determine the 2D projected structures of adlayers of dimensions incommensurate with that of the substrate.

In contrast, the method we have developed period [6, 7, 8, 9] determines the phases to both measured CTRs and superstructure rods (SRs). By subtracting the contributions to the CTRs from the (known) bulk structure, it is possible to obtain a 3D distribution of phased structure factors of the surface unit cell, an inverse Fourier transform of which reveals the entire 3D structure of the surface unit cell.

2. Methodology

a. Basic algorithm

The diffraction of collimated x-rays from a three- dimensional macroscopic crystal results in the formation of Bragg spots on a distant detector. Regarded as a function of the momentum transfer vector $\mathbf{q}=\mathbf{k}-\mathbf{k}_0$, where $\mathbf{k}_0$ and $\mathbf{k}$ are wavevectors of the incident and scattered x-rays, the diffracted intensities may be associated with a set of points in reciprocal space constituting a reciprocal lattice related to translational symmetry vectors in real space.

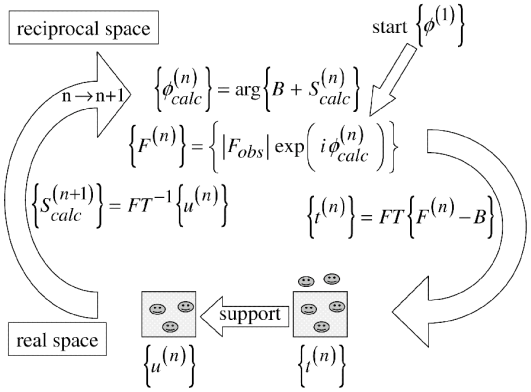

Fig. 1 Schematic flowchart of iterative phase recovery algorithm described in text.

In x-ray diffraction from a crystal surface (regarded as an entity of two-dimensional periodicity in directions parallel to the surface), the breaking of the crystal periodicity perpendicular to the surface broadens the Bragg spots into streaks in directions perpendicular to the surface in reciprocal space, referred to as *crystal truncation rods* (CTRs) [10, 11]. If the surface is reconstructed, that is if the outermost atomic layers have a different (usually larger) 2D unit cell compared to the deeper (bulk) layers, the diffraction conditions give rise to extra reciprocal-lattice rods known as *superstructure rods* (SRs). A SXRD experiment is capable of measuring the intensities along each of these types of rods as functions of reciprocal-space coordinates.

The aim of surface crystallography is the determination of the atomic structure of the surface layers insofar as they differ from the bulk. The bulk structure is normally known. We have developed a direct method for SXRD that takes as input only measured intensities of CTRs and SRs and a knowledge of the bulk structure, and gives as output the 3D electron density of an entire surface unit cell, where the thickness of this cell extends to a depth where the structure is indistinguishable from that of the bulk.

Our scheme employs an iterative algorithm that alternately satisfies constraints in real and reciprocal space [12], and is illustrated in Fig. 1. From the measured intensities, it is possible to find the amplitudes, $\left|F_{hkl}^{(obs)}\right|$ as a function of the Miller indices (h,k,l) associated with the momentum transfer vector

$$\mathbf{q} = h\mathbf{b}_1 + k\mathbf{b}_2 + l\mathbf{b}_3 \ , \tag{1}$$

where $(\mathbf{b}_1,\mathbf{b}_2,\mathbf{b}_3)$ are basis vectors of a reciprocal lattice defined with respect to the bulk real space lattice. At any particular iteration, n, say, the combination of the observed amplitudes and assigned phases gives the current estimate of (target) surface structure factors T consistent with the experimental data, namely:

$$T_{hkl}^{(n)} = f^{(n)}\left|F_{hkl}^{obs}\right|\exp\left\{i\phi_{hkl}^{(n)}\right\} - B_{hkl} \tag{2}$$

where B_{hkl} represents the corresponding (calculable) structure factor of the known bulk crystal. For the SRs, of course, $B_{hkl} = 0$. For the CTRs, the phases $\phi_{hkl}^{(n)}$ are assigned those of the calculated structure factors at the previous iteration *via*

$$\phi_{hkl}^{(n)} = \arg\left\{F_{hkl}^{(n-1)}\right\} \tag{3}$$

where

$$F_{hkl}^{(n-1)} = B_{hkl} + S_{hkl}^{(n-1)}, \tag{4}$$

where $S_{hkl}^{(n-1)}$ is the theoretical estimate of the surface structure factor from the previous iteration. At the initial (n=1) iteration, we take $S_{hkl}^{(0)} = 0$ for all (hkl). For the SRs the initial phases $\phi_{hkl}^{(0)}$ may be assigned random numbers. The scaling factor $f^{(n)}$ in (2) is defined by the least-squares criterion

$$\frac{dR^{(n)}}{df^{(n)}} = 0 \tag{5}$$

where

$$R^{(n)} = \sum_{hkl} \left\{ \left| F_{hkl}^{(n-1)} \right| - f^{(n)} \left| F_{hkl}^{obs} \right| \right\}^2 \tag{6}$$

which yields

$$f^{(n)} = \frac{\sum_{hkl} \left| F_{hkl}^{(n-1)} \right\| F_{hkl}^{obs} \right|}{\sum_{hkl} \left| F_{hkl}^{(obs)} \right|^2} \quad . \tag{7}$$

The Fourier transform

$$t^{(n)}(x,y,z) = \sum_{hkl} T_{hkl}^{(n)} \exp\left\{ -2\pi i \left(hx + ky + lz \right) \right\}, \tag{8}$$

where x, y, and z are fractional coordinates in the directions of basis vectors $\mathbf{a}_1, \mathbf{a}_2$ and $\mathbf{a}_3$ of the bulk unit cell ($\mathbf{a}_1$ and $\mathbf{a}_2$ taken parallel to the surface, and $\mathbf{a}_3$ perpendicular to it), gives the current estimate of the electron density of the surface unit cell. With these definitions, the CTRs correspond to integer values of h and k, while SRs are labeled by fractional values of one or both of these Miller indices. The breaking of the periodicity in the direction normal to the surface gives rise to measurable scattered intensity for a continuous range of values of the third Miller index l.

The expression (8) may be regarded as a current estimate of the electron density of the parts of the surface that differ from that of the bulk. That is, it represents an estimate of the electron density associated with any adsorbates and/or any parts of the substrate undergoing relaxation and/or reconstruction. The values of h and k entering into the summation (8) are those integer and fractional values corresponding to the measured CTRs and SRs. A conventional fast Fourier transform (FFT) would automatically generate a set of values of $t^{(n)}(x,y,z)$ on a grid of points in real space whose lateral extent is that of the surface unit cell (which may be larger than the bulk unit cell). However, since the scattered intensities vary as a continuous function of l, the intervals Δl between successive measurements of the structure factors are somewhat arbitrary. The range of z-values for which the surface electron density $t^{(n)}(x,y,z)$ is calculated by a FFT is $a_3/(\Delta l)$. This range may be substantially greater than the physical extent of the surface unit cell. In that case, it might be said that the structure factors are *oversampled* [13] in the direction of Miller index l with respect to the corresponding dimension of the object to be recovered.

This allows us the opportunity to obtain a revised estimate $u^{(n)}(x,y,z)$ of the surface electron density by making it conform to object domain constraints, e.g., by operations of the form [14]

$$u^{(n)} = \begin{cases} t^{(n)}, \{x,y,z\} \notin \gamma \\ 0, \{x,y,z\} \in \gamma \end{cases} \qquad (9)$$

where γ represents the set of points that do not satisfy the constraints. In our case, we take γ to represent the region of space not expected to contain surface electron density. If Δl is sufficiently small, this may even be the majority of the range of values of z. It should be noted that although these *support constraints* in real space may be the simplest form of object domain operations (ODOs) and the ones we have used primarily in our SXRD work, they are far from the only such form of constraints that can be used. In fact, Fienup suggested at least four other forms of types of ODOs, which gave rise to algorithms that he termed *error reduction*, *basic input-output, output-output, and hybrid input-output* algorithms. It is possible that different forms of ODOs are suited to different kinds of phasing problems. Indeed Fienup has pointed out [14] that using one form, e.g. the error-reduction algorithm, in the initial stages, followed by another, e.g. the hybrid input-output one, at a later part of the phasing process may be advantageous in some cases. We have also suggested and proved the viability of yet another form of ODOs, based on Collins' maximum entropy algorithm [15] that we have generalized also to the phasing problem of low energy electron diffraction (LEED) [16, 17].

We can now obtain a revised estimate of the theoretical surface structure factors by the Fourier transform

$$S_{hkl}^{(n)} = \sum_{x,y,z} u^{(n)} \exp\{2\pi i(hx + ky + lz)\} \quad . \qquad (10)$$

Incrementing n by 1, new estimates of the phases of all the structure factors may be recalculated by (4) and (3), and together with a revised calculation of the scaling factor from (7), a new estimate of the (experimental) surface structure factors may be computed from (2) and the entire cycle repeated until convergence in the surface electron density $u(x,y,z)$. Peaks in this distribution would be expected to reveal the positions of atoms in the surface unit cell.

The possibility of inverting a set of oversampled Fourier amplitudes (without phases) depends on the dimensionality: There is no unique solution in 1D [18], but it has been argued that one may be found if oversampling is possible in 2D and 3D [19, 20]. In the seminal works [12, 13], the object recovered was a 2D projection of 2 non-periodic dimensions. In recent work using electron diffraction [21], the 2D projection of a carbon nanotube, of one periodic and one non-periodic dimension, was recovered using oversampling methods. Our work has shown that it is possible to recover a 3D object with just one non-periodic dimension available for oversampling. Diffraction from a system with 2D periodicity (such as a crystal surface) gives rise to multiple rods; we suggest that although there is only one oversampled dimension, the many rods sampled constitute many interdependent, 1D Fourier transforms, and a unique phase solution exists.

b. Extension to LEED

One way to understand our inversion algorithm for SXRD is in terms of a holographic analogy. Every measured data point may be regarded as the square modulus of a complex quantity that may be regarded as a linear combination of a complex scattered amplitude from a known part of the sample (generally the surface-truncated bulk) which may be regarded as a *reference* "wave", and that from the unknown, surface part of the structure, regarded as an *object* "wave". During holographic reconstruction, the complex object wave is recovered from the measured intensity data and a knowledge of the reference wave. In SXRD, the quantity of interest is not the object wave, but the electron density of the unknown part of the structure (usually the surface region). Due to the single-scattering approximation, that is usually valid for x-ray scattering by atoms, the complex object wave is related to this electron density by a Fourier transformation. Since this is an invertible operation, the current estimate of electron density may be recovered by an inverse Fourier transform from the current estimate of the object wave, itself found from the holographic reconstruction. The current estimate of the electron density is then updated by ODOs, used to calculate a theoretical estimate of the object wave, and hence a guesses of the phases of the measured amplitudes and the entire cycle repeated.

During the grant period, one of us (DKS) addressed also the even more challenging inverse problem of low-energy electron diffraction (LEED), a classic case of strong multiple scattering. It was shown that even this problem may, to a good approximation, be cast in the same general framework as above: the measured intensities may be regarded as square moduli of sums of reference and object wave contributions. Once again, the reference wave is defined as the complex amplitude scattered from the known part of the structure (the bulk). Since this structure is known, this amplitude may be calculated exactly, *including all multiple-scattering*. It is also necessary to generalize the definition of the object wave. To a good approximation, the latter may be regarded as a linear combination of *elementary object waves* (in SXRD these are just exponential factors) calculated by summing all multiple scattering paths between adatoms at a test positions and the bulk. With these definitions, and a prior calculation of the reference amplitudes by a multiple-scattering computer program, the complex object wave may be recovered by exactly the same holographic reconstruction algorithm as SXRD. The aim of the inverse method is the recovery of the spatial distribution of adatoms on the surface. This distribution may be regarded as the set of coefficients of the linear combination of elementary object waves (also calculated by a multiple-scattering program) that constitutes the total object wave. Since this object wave is calculated by the holographic reconstruction algorithm, the sole remaining problem is the determination of the coefficients of this linear expansion. We have shown how this may be done by a generalization of our maximum entropy method for SXRD [16, 17]. In more recent (unpublished) work, we have also shown current estimates of a real space distribution of adatoms may be recovered from a set of complex object waves by matrix inversion using the singular value decomposition (SVD) method. This distribution may be updated in real space in the usual way by appropriate ODOs in essentially the same iterative algorithm that alternately satisfied constraints in real and reciprocal space. This may be regarded as a rare solution of a *multiple-scattering* inverse problem

3. Implementations

A key feature of the previous award and of the present proposal is the synergy of the efforts on the theoretical and experimental fronts. Here, we briefly report progress in two areas that serve to illustrate this beneficial interplay.

a. multiple domains

A surface unit cell need not have the symmetry of the substrate, provided there are multiple surface domains related by substrate symmetry operations. The existence of multiple domains complicates our attempts to recover the phases of the structure factors: although the SRs may arise separately from the different domains, more than one domain may contribute to each the integer-order rods. However, since the structure factors of the different domains are related by symmetry, it is possible to find the expression for the amplitude of a structure factor from a single domain in terms of the measured structure factor and the current estimate of the surface electron density. Making use of this relationship, the algorithm in section II.A.2 may be modified to determine the surface structure of each individual domain [8]. We have successfully used this modified algorithm to determine a multi-domain structure from experimental data [**Error! Bookmark not defined.**].

b. guiSXRD

Under the auspices of the original award, a powerful and flexible environment for analysis of SXRD data has been developed, which we call guiSXRD (graphical user inteface for SXRD). The suite automates many of the routine tasks required to reduce SXRD data, yet still allows the user fine control over the results. It is cross-platform compatible since it is written using MatLab; we routinely use it on Windows, Linux/Unix, and MacOS machines.

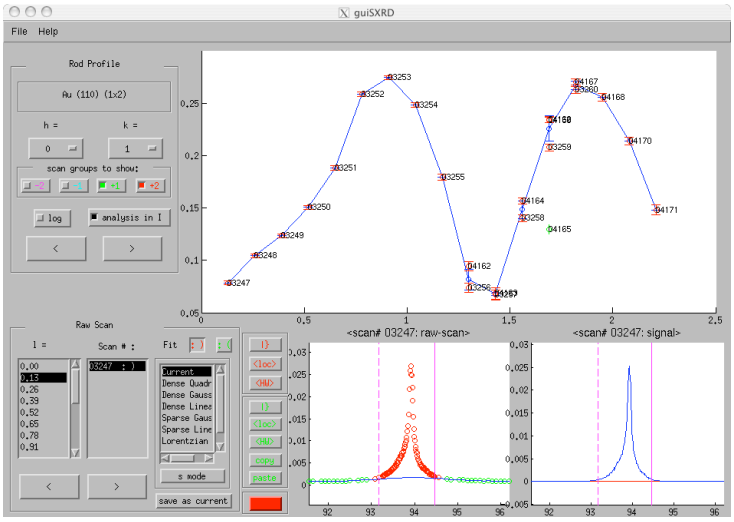

Fig. 2 (color) Screen shot of guiSXRD data analysis tool developed to automate SXRD data reduction.

The software suite allows one to import data from the beamline control software (typically SPEC), automatically fit each scan, and extract an intensity. Appropriate geometrical and polarization corrections are made to render the structure factor. The program organizes the data by *hkl* value and averages equivalent reflections based on the symmetry of the substrate. A screen shot of a typical session is shown in Fig. 2. The top panel shows the structure factors along a CTR or SR, and the bottom panels display the fitting of an individual scan. The suite is freely distributed and fully documented at:

http://hermes.phys.uwm.edu/~russell/projects/guiSXRD/index.html.

B. Progress on Experimental Systems

We have experimentally investigated a number of surface systems during the grant period, and have obtained gratifying success in recovering their electron density. Here, we show results for three related systems: the well-known clean Au(110)-(2×1) [**Error! Bookmark not defined.**], and two heretofore unknown Sb-induced reconstructions, namely, Sb/Au(110)-*c*(2×2) [**Error! Bookmark not defined.**] and Sb/Au(110)-($\sqrt{3}\times\sqrt{3}$)R54.7°[**Error! Bookmark not defined.**]. We chose the clean Au(110) surface as a test system to establish the efficacy of our technique, and then demonstrated the method's utility in solving two new surfaces. These data were acquired using beamline X22C at the NSLS (owned by the Physics Department of BNL), which has an endstation that is well-suited to probe the surfaces of metals.

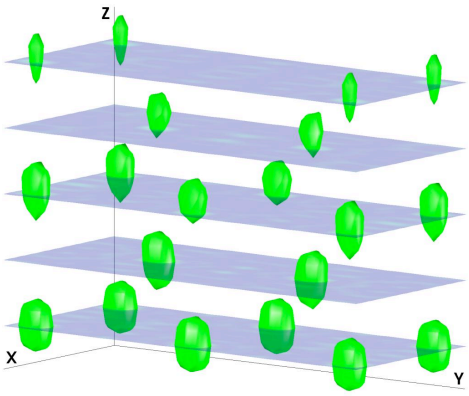

Fig. 3 (color) Perspective view of isosurfaces of recovered electron density for clean Au(110)-(2×1).

1. Clean Au(110)-(2×1)

The clean surface of Au(110) undergoes a missing-row reconstruction. The principal structural feature is that every other row of close-packed atoms along the $[1\bar{1}0]$ direction is missing, thereby doubling the unit cell in the $[001]$ direction [22]. Also, this surface exhibits an oscillatory relaxation, with a contraction in the first-second layer spacing, and a slight expansion in the second-third layer spacing. [23, 24, 25]. In addition, the corrugation of the surface due to the missing rows causes distortions in the

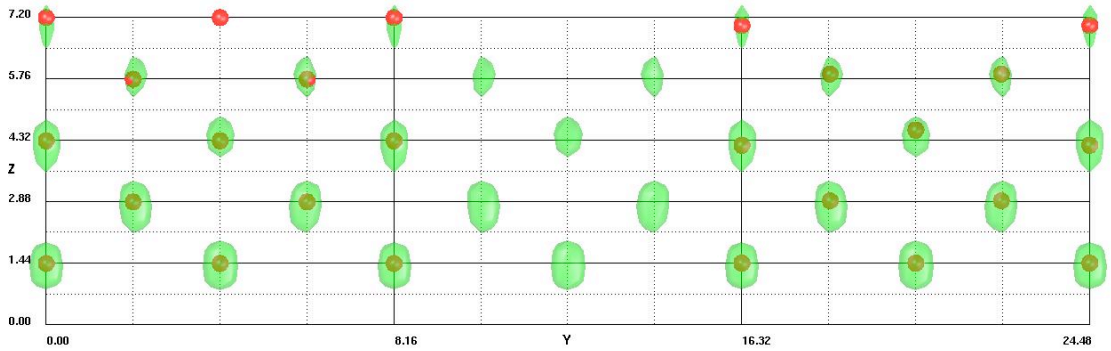

Fig. 4 (color) Side-view orthographic projection of isosurfaces (green) of recovered charge density for clean Au(110)-(2×1). The unit cell is repeated three times. On the left, the red spheres are located at bulk-terminated positions. On the right, the red spheres are positioned according to conventional χ^2 fitting.

underlying layers; consistent with the symmetry of the surface, a pairing along the $[001]$ direction has been reported for the second [23,25] and fourth layers [25], while a buckling has been reported in the third layer [23,24].

After acquiring a complete SXRD data set, our direct algorithm (Sec. A.2) was applied to the data. Convergence was typically reached in < 40 iterations. Trials were initiated with random initial phases, but always converged to the same recovered electron density. The results are shown in Figs. 3 and 4, which depict isosurfaces of recovered electron density. The principal structural feature of the surface reconstruction, the missing row in the first layer, is obvious in the recovered electron density. Also, the relaxation of the top layer is clearly evident in Fig. 4, as judged by the inward displacement of the remaining electron density compared to the bulk-terminated positions. Moreover, subtler features of the surface structure, such as subsurface relaxation, pairing, and buckling, are also evident upon closer inspection. Notice that the electron density maxima in the second layer are displaced toward the center of the cell compared to the bulk-positioned spheres; this observation is consistent with the SXRD study of Ref. [25] that observed pairing in the second and fourth layers. Also, note the density maxima in the third layer are displaced alternately inward and outward compared to the bulk-positioned spheres, consistent with the third-layer buckling observed in previous work [23, 24]. Beyond these naked-eye findings, we can conduct conventional χ^2 refinement of the atomic positions using the electron density

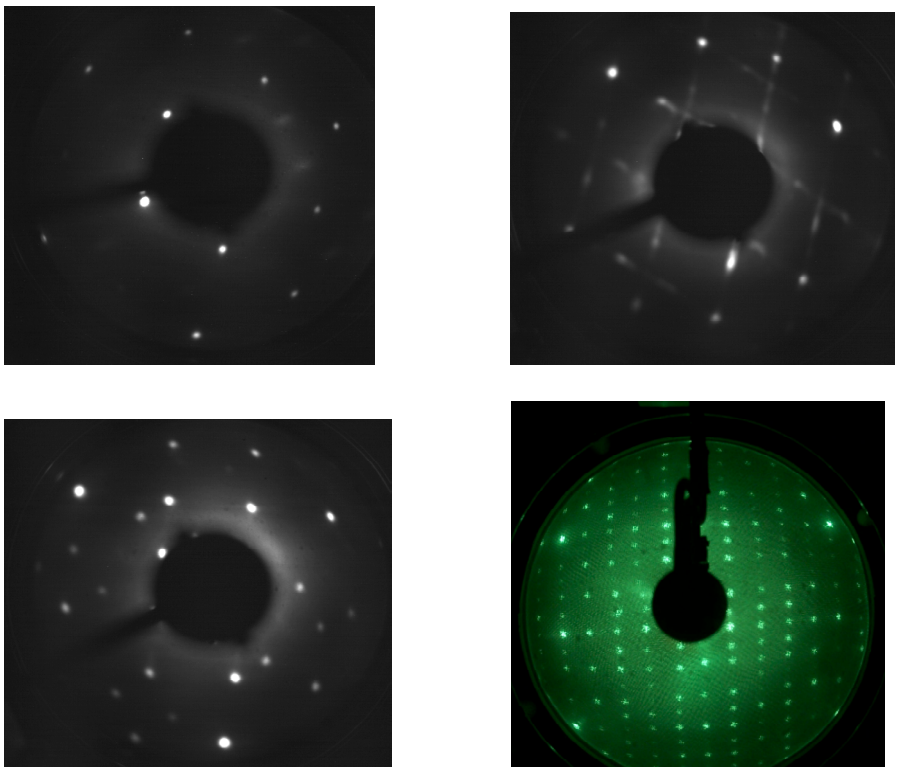

Fig. 5 LEED patterns recorded for Sb/Au(110)-c(2×2) (top left), intermediate (top right), (√3×√3)R54.7° (bottom left), and p(5×6) (bottom right).

maxima as starting positions; results were completely consistent with the consensus of previous measurements, including pairing and buckling in layers one to four, and yielded an acceptable χ^2 of 2.0.

2. Sb/Au(110)-c(2×2)

After this successful demonstration on a test system with a known structure, we applied this method to uncover the structure of several heretofore-unknown surface phases. Due to the low solid solubility of Sb in Au, and the fact that they form an ordered compound ($AuSb_2$) in the bulk, we decided to examine the adsorption of Sb on Au(110). We discovered at least three new surface phases that had never been reported in the literature previously. Using LEED, we tracked changes in the long-range order with Sb coverage, as shown in Fig. 5. Upon inital adsorption of Sb, the (2×1) pattern of the clean surface begins to dim, and at ~0.3 ML Sb coverage, *c*(2×2) diffraction spots appear in the center of the 2D unit cell. Upon further deposition, i.e., in excess of 0.5 ML, the *c*(2×2) diffraction spots split into four, which move continuously towards the corners of the (1×1) unit cell. Upon reaching approximately 0.80 ± 0.15 ML Sb coverage, the superstructure spots "lock in" to form a Sb/Au(110)-$\left(\sqrt{3}\times\sqrt{3}\right)R54.7^\circ$ pattern. Finally, upon deposition of additional Sb, a *p*(5×6) pattern emerges. We have made structural determinations of two of these phases, described briefly here.

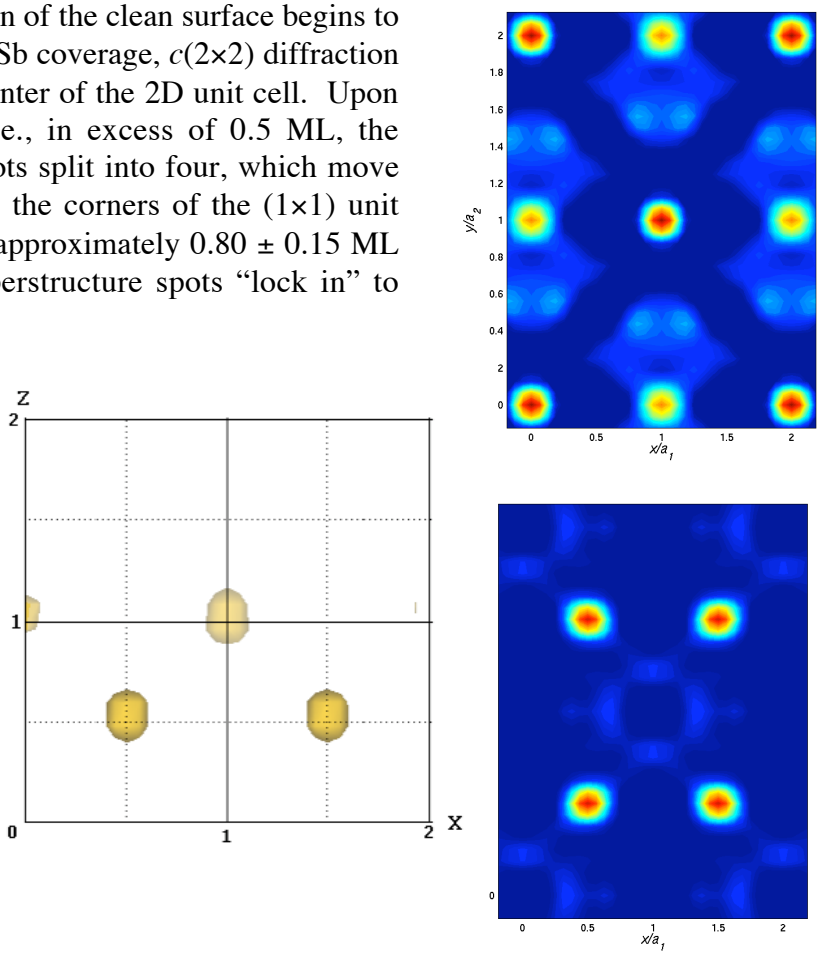

Fig 6 (color) Depictions of recovered electron density for Sb/Au(110)-c(2×2) surface. Left panel shows side-view orthographic projection and right panel shows top-view 2D cuts through surface layer (top) and second atomic layer (bottom).

As there have been no previous reports of the 0.5 ML Sb / Au(110)-*c*(2×2) phase,

no model structures were available to compare our scattering data against. The Patterson function (not shown) had only one strong interatomic vector within the (2×2) unit cell, namely, $(\mathbf{a}_1+\mathbf{a}_2)$, where $\mathbf{a}_1$ and $\mathbf{a}_2$ are the basis vectors for the (1×1) unit cell. The vector $(\mathbf{a}_1+\mathbf{a}_2)$ links every other high-symmetry atomic site, as on a chessboard. Together with the observation that the surface has a coverage of $\theta_{Sb} \approx 0.5$ ML, one is tempted to conclude that the surface can simply be described by Sb occupying every other atop, long bridge, short bridge, or hollow site, in a chessboard fashion. Note that the Patterson function alone cannot distinguish these possibilities. However, we were able to infer what turned out to be the correct surface model by examining the output of our direct algorithm (Sec. A.1), shown in Fig. 6. The recovered electron density revealed that there were atoms occupying not just every *other* surface hollow site, but all such sites. However, the charge density in half the sites is greater than in the other half. (See Fig. 5.) Thus, we identify a model where every other hollow site is occupied by Au adatoms, while the remaining half is occupied by Sb adatoms.

Conventional χ^2 fitting to the model so suggested revealed quantitative agreement with the scattering data, as detailed in Ref [26]. A reduced χ^2 of 0.90 was reached with very reasonable values of the structural parameters, allowing us to conclude with certainty that our direct algorithm accurately visualized the charge density in the near-surface region for this heretofore unknown surface phase.

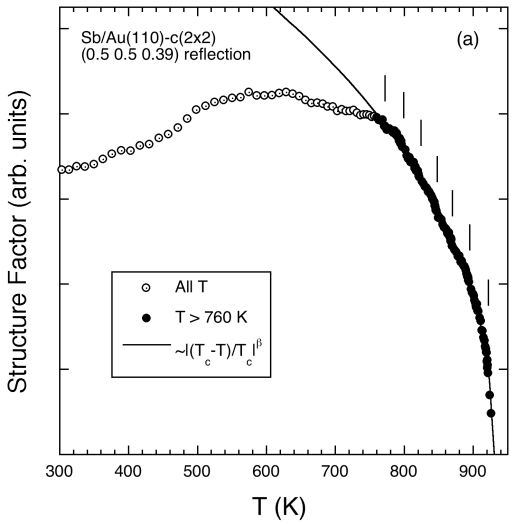

Fig. 7 Square root of fractional-order reflected intensity vs. T indicating critical behavior.

Studies were also undertaken to monitor the thermal stability of this surface. The order of the $c(2\times2)$ phase during heating was monitored by examining the Bragg component of the $\left(\frac{1}{2}\frac{1}{2}0.39\right)$ reflection. We found that the reconstruction persisted to surprisingly high temperatures. Fig. 7 displays the square root of the peak intensity, which is proportional to the structure factor F, of this reflection as a function the substrate temperature T. It is evident that the structure factor initially *increases* upon heating up to about 600 K, before falling dramatically as the substrate temperature exceeded 800 K. Nevertheless, there is still significant intensity at 900 K. The behavior of the decrease of the structure factor within about 150 K of this temperature is reminiscent of that associated with a phase transition. Consequently, data points for $T > 760$ K (filled circles in Fig. 10) were fit to a function of the form $F = At^{\beta}$, where the reduced temperature $t = \left|(T_c - T)/T_c\right|$. The best fit renders an estimate of the critical exponent β and the critical temperature T_c. While a power law dependence on the reduced temperature t is expected in critical theory only for temperatures just below the critical temperature, there is no single criterion for determining the correct range. Consequently, fits were made to the data using a variety of lower bounds on the fitted temperature, and the variation in the

best-fit parameters was used to estimate their uncertainty. Acceptable fits were found for minimum temperatures of 750 to 870 K, and we thereby determined values for the critical exponent β of 0.40 ± 0.05 and for the critical temperature T_c of 928 ± 4 K. For comparison, the bulk melting point of $AuSb_2$ is 732 K. The process was reversible upon cooling; the peak re-emerged just above 900 K, and grew in intensity upon cooling, recovering essentially all of its intensity by 780 K. We also monitored the width of this reflection by acquiring ω scans at the positions indicated by the vertical lines in Fig. 10. The width stayed essentially unaltered, indicating no observable change in the correlation length of the long-range order.

3. Sb/Au(110)-$\left(\sqrt{3}\times\sqrt{3}\right)R54.7°$

Further along the rich phase diagram we discovered for Sb adsorption on Au(110) lies the Sb/Au(110)-$\left(\sqrt{3}\times\sqrt{3}\right)R54.7^\circ$ phase. Again, upon adsorption of Sb in excess of 0.5 ML, the $c(2\times2)$ diffraction spots in the center of the 2D unit cell split into four, which move continuously towards the corners of the (1×1) unit cell. Upon reaching approximately 0.80 ± 0.15 ML Sb coverage, the superstructure spots "lock in" to positions at $\left(\frac{m}{3},\frac{n}{3}\right)$, where $m, n = 1$ or 2 (for the first Brillouin zone). These locations are consistent with two domains, each of which has lattice vectors that are $\sqrt{3}$ larger than the corresponding bulk vector, and rotated by 54.7°. Thus, we identify the new phase as Sb/Au(110)-$\left(\sqrt{3}\times\sqrt{3}\right)R54.7^\circ$ in the Wood notation. Considering the size of the new unit cell, and the error bars in the Sb coverage measurement, it seems likely that the ideal Sb coverage is 2/3 ML. Note that the surface stoichiometry so obtained is the same as in the bulk compound $AuSb_2$.

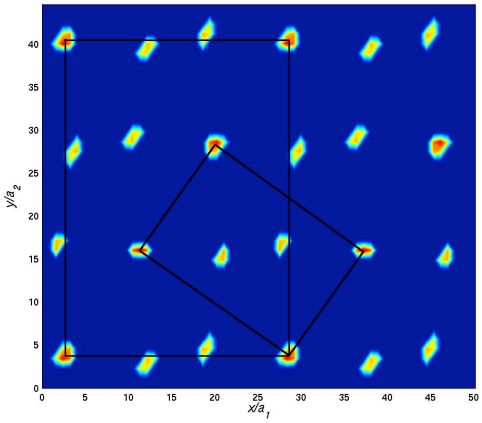

Fig. 8 (color) Top-view 2D cut though surface plane of recovered electron density from a single surface domain of Sb/Au(110)-(√3×√3)R54.7°. Both (3×3) and (√3×√3)R54.7° unit cells are shown.

Again, an extensive data set of regularly-spaced structure factors was acquired at Beamline X22C at the NSLS. Using the improvements to the code to account for multiple domains described above, the algorithm recovered a visualization of the near-surface electron density of a single surface domain shown in Fig. 8. Once again, the algorithm reveals surface atoms occupying hollow sites with two different magnitudes of electron density. Again, they are easily interpretable as arising from Sb and Au atoms; in this phase, they have coverages of 2/3 and 1/3 ML, respectively. Au atoms occupy every third row of hollow sites along the diagonal, while Sb atoms occupy the intervening two rows. Initial conventional fitting to this model resulted in χ^2 value of ~1.8, which indicates that this

model is very likely to be correct. After refining the structural parameters of this fit, we find the Sb atoms are displaced slightly away from the hollow sites toward the nearest Au rows, as shown in Fig. 9. This work is detailed in Ref. 27.

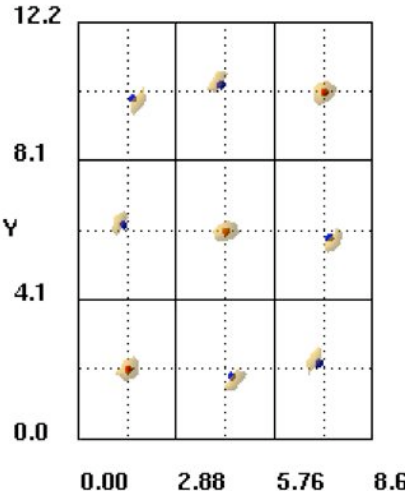

Fig. 9 (color) Top-view orthographic projection of isosurfaces of recovered electron density for Sb/Au(110)-(√3×√3)R54.7°. The red and blue spheres represent Au and Sb positions, respectively, derived from χ^2 fitting.

Moreover, it is now possible to readily understand the evolution of the LEED patterns shown in Fig. 5. In the language just used here, the $c(2\times2)$ structure has every other diagonal row of hollow sites occupied by Sb and the other rows occupied by Au. Upon adding more Sb to this structure, it is evidently accommodated by occupying another diagonal row, which is bordered by an Au row on one side and an Sb row on the other. In other words, an antiphase domain boundary (APB) is introduced between $c(2\times2)$ regions, allowing an additional Sb row to be accommodated at the boundary. As more and more Sb is introduced, these APBs become more and more prevalent. If the APBs are regularly spaced, a series of diffraction spots would be apparent along the diagonal of the Brillouin zone; however, a distribution of such APBs results in smeared out intensity along the diagonal [28], consistent with our LEED patterns of Fig. 5. Finally, at 2/3 ML, two of every three rows are occupied by Sb, and no more can be accommodated without having three adjacent Sb rows. Evidently, the structure is stabilized in this configuration.

Summary

During the tenure of the award, we have made significant progress on implementing and refining a robust direct method algorithm for determining atomic locations from surface x-ray diffraction. We have demonstrated the efficacy of this method on real experimental data, both by demonstration efforts on a known reconstructed surface and by unraveling the structure of heretofore unknown surface systems.

Finally, significant efforts on disseminating these ideas have begun. There is a looming crisis in surface x-ray diffraction: although better x-ray sources and detectors have allowed extensive datasets from complex surface systems to be acquired in reasonable times, analytical methods have not kept pace. The result is that the bottleneck in many cases is the analysis of these complex datasets, not their acquisition. Lyman was invited to speak at a workshop on the future of surface x-ray diffraction at the Advanced Photon Source, and the method presented was well received. As a result, a collaborative effort has been established with workers at the Swiss Light Source, in an effort to interpret their excellent, but complex, datasets from complex oxide systems.

C. Papers Acknowledging DOE Support During Award Period

1. "Solution of a multiple-scattering inverse problem: electron difraction from surfaces," D. K. Saldin, A. Seubert, and K. Heinz, *Phys. Rev. Lett.* **88**, 115507 (4 pages) (2002).

2. "Surface crystallography by alternating constraints in real and reciprocal space: case of mixed domains," D. K. Saldin, R. J. Harder, V. L. Shneerson, and W. Moritz, Invited paper, VIIth European Conf. on Surface Crystallography and Dynamics, Leiden, The Netherlands, August 2002, *J. Phys.: Condens. Matter* **14**, 4087-4100 (2002).

3. "Direct determination by low energy electron diffraction of the atomic structure of surface layers on a known substrate," A. Seubert, K. Heinz, and D. K. Saldin, *Phys. Rev. B* **67**, 25417 (11 pages) (2003).

4. "Surface structure solution by x-ray diffraction: structure completion with positivity and atomicity constraints," D. K. Saldin, V. L. Shneerson, and R. Fung, Invited paper, 7th Int. Conf. on Surface X-ray and Neutron Scattering (7SXNS), Lake Tahoe, California, September 2002, *Physica B* **336**, 16-26 (2003).

5. "Holographic surface crystallography: substrate as reference," R. J. Harder and D. K. Saldin, Invited paper, in *Solid State Photoemission and Related Methods* , pp. 370-386. Edited by W. Schattke and M. A. Van Hove (Wiley-VCH, Weinheim, 2003).

6. "Atomic-scale visualization of surfaces with x rays," P.F. Lyman, V.L. Shneerson, R. Fung, R.J. Harder, E.D. Lu, S.S. Parihar, and D.K. Saldin, *Phys. Rev. B* **71**, 081402(R)-1-4 (2005).

7. "Structure and stability of Sb/Au(110)-*c*(2×2) surface phase," P.F. Lyman, V.L. Shneerson, R. Fung, S.S. Parihar, H.T. Johnson-Steigelman, E.D. Lu, and D.K. Saldin, *Surf. Sci.* **600**, 424-435 (2006).

8. "Phase and Amplitude Recovery and Diffraction Image Generation Method: structure of Sb/Au(110)-($\sqrt{3}\times\sqrt{3}$)*R*54.7° from surface x-ray diffraction," R. Fung, V.L. Shneerson, P.F. Lyman, S.S. Parihar, H.T. Johnson-Steigelman, and D.K. Saldin, submitted to *Acta Cryst. A*.

D. Graduate Students Supported

During the grant period, three graduate students have received partial support from this award. Ross Harder, who completed his Ph.D. in May 2002 and is currently

working as a postdoc with Prof. Ian K. Robinson, contributed to the early stages of the project; he is an author on publications 2, 5, and 6 above. Russell Fung, who joined the UWM Physics Department in Aug. 2002, has been the main contributor to the theoretical effort. He has been an outstanding student, and is co-author of publications 4, 6, 7, and 8 above. He defended his Ph.D. Dissertation in Fall 2005. Somendra Parihar joined the UWM Physics Department in 2002, and has been the main contributing student on the experimental side. He has completed his Ph.D. qualifying examinations, and is currently conducting his dissertation research. He is a co-author on 6, 7, and 8 above.

In addition, two postdoctoral associates, Dr. Valentin Shneerson and Dr. Erdong Lu, have received minor support from the award. They had each been working on related projects, and were supported for short periods to allow them to make key contributions to the publications above. Shneerson is a co-author on publications 2, 4, 6, 7, and 8, while Lu is a co-author on 6 and 7 above.

References

1 Y. Yacoby, R. Pindak, R. MacHarrie, L. Pfeiffer, L. Berman, and R. Clarke, "Direct structure determination of systems with two-dimensional periodicity," J. Phys.: Condens. Matter **12**, 3929-3938 (2000).

2 M. Sowwan, Y. Yacoby, J. Pitney, R. MacHarrie, M. Hong, J. Cross, D.A. Walko, R. Clarke, R. Pindak, and E.A. Stern, "Direct atomic structure determination of epitaxially grown films: Gd_2O_3 on GaAs(100)", Phys. Rev. B **66**, 205311-1-12 (2002).

3 J. Rius, C. Miravitlles, R. Allmann, "A tangent formula derived from Patterson-function arguments .4. The solution of difference structures directly from superstructure reflections," Acta Crystallogr. A **52**, 634-639 (1996).

4 J. Rius, X. Torrelles, C. Miravitlles, J.M. Amigo, M.M. Reventos, "A new interpretation and practical aspects of the direct-methods modulus sum function. VIII," Acta Crystallogr. A **58**, 21-26 (2002).

5 X. Torrelles, J. Rius, A. Hirnet, W. Moritz, M. Pedio, R. Felici, P. Rudolf, M. Capozi, F. Boscherini, S. Heun, B.H. Mueller, and S. Ferrer, "Real examples of surface reconstructions determined by direct methods," J. Phys." Condens. Matter **14**, 4075-4086 (2002).

6 D.K. Saldin, R. Harder, H. Vogler, W. Moritz, and I.K. Robinson, "Solving the structure completion problem in surface crystallography", Comput. Phys. Commun. **137**, 12-24 (2001).

7 D.K. Saldin, R. J. Harder, V.L. Shneerson, and W. Moritz, "Phase retrieval methods for surface x-ray diffraction", J. Phys.: Condens. Matter **13**, 10689-10707 (2001).

8 D.K. Saldin, R. J. Harder, V.L. Shneerson, and W. Moritz, "Surface x-ray crystallography with alternating constraints in real and reciprocal space: the case of mixed domains", J. Phys.: Condens. Matter **14**, 4087-4100 (2002).

9 D.K. Saldin, V.L. Shneerson, and R. Fung, "Surface structure solution by x-ray diffraction: structure completion with positivity and atomicity constraints", Physica B **336**, 16-26 (2003).

10 S.R. Andrews and R. A. Cowley, "Scattering of x-rays from crystal surfaces," J. Phys. C **18** 6427-6439 (1985).

11 I.K. Robinson, "Crystal truncation rods and surface roughness," Phys. Rev. B **33**, 3830-3836 (1986).

12 J. R. Fienup, "Reconstruction of an object from modulus of its Fourier transform," Optics Lett. **3**, 27-29 (1978).

13 J.W. Miao, P. Charalambous, J. Kirz, and D. Sayre, "Extending the methodology of x-ray crystallography to allow imaging of micrometre-sized non-crystalline specimens," Nature (London) **400**, 342-344 (1999).

14 J.R. Fienup, "Phase retrieval algorithms: a comparison", Appl. Opt. **21**, 2758 (1982).

15 D.M. Collins, "Electron density maps from imperfect data by entropy maximization", Nature (London) **298**, 49 (1982).

16 D.K. Saldin, A. Seubert, and K. Heinz, "Solution of a multiple-scattering inverse problem: Electron diffraction from surfaces," Phys. Rev. Lett. **88**, 115507-1-4 (2002).

17 A. Seubert, K. Heinz, and D.K. Saldin, "Direct determination by low-energy electron diffraction of the atomic structure of surface layers on a known substrate," Phys. Rev. B **67**, 125417-1-11 (2003).

18 A. Walther, "The question of phase retrieval in optics," Opt. Acta **10**, 41-49 (1963).

19 R.H.T. Bates, "Fourier phase problems are uniquely solvable in more than one dimension. I: Underlying theory," Optik (Stuttgart) **61**, 247-262 (1982).

20 R. Barakat and G. Newsam, "Necessary conditions for a unique solution to two-dimensional phase recovery," J. Math. Phys. **25**, 3190-3193 (1984).
21 J.M. Zuo, I. Vartanyants, M. Gao, R. Zhang, and L.A. Nagahara, "Atomic resolution imaging of a carbon nanotube from diffraction intensities," Science **300**, 1419-1421 (2003).
22 W. Moritz and D. Wolf, "Structure determination of the reconstructred Au(110) surface," Surf. Sci. **88**, L29-L34 (1979).
23 W. Moritz and D. Wolf, "Multilayer distortion in the reconstructed (110) surface of Au," Surf. Sci. **163**, L655-L665 (1985).
24 M. Copel and T. Gustafsson, "Structure of Au(110) determined with medium-energy ion scattering," Phys. Rev. Lett. **57**, 723-726 (1986).
25 E. Vlieg, I. K. Robinson, and K. Kern, "Relaxations in the missing-row structure of the (1×2) reconstructed surface of Au(110) and Pt(110)," Surf. Sci. **233**, 248-254 (1990).
26 P.F. Lyman, V.L. Shneerson, R. Fung, S.S. Parihar, H.T. Johnson-Steigelman, E.D. Lu, and D.K. Saldin, "Structure and stability of Sb/Au(110)-*c*(2×2) surface phase," Surf. Sci.**600**, 424-435 (2006).
27 R. Fung, V.L. Shneerson, P.F. Lyman, S.S. Parihar, H. T. Johnson- Steigelman, and D.K. Saldin, **"**Phase and Amplitude Recovery and Diffraction Image Generation Method: Structure of Sb/Au(110)-($\sqrt{3}\times\sqrt{3}$)R54.7° from Surface X-ray Diffraction," submitted to Acta Crystallographica.
28 V. Maurice, J. Oudar, and M. Huber, "Sulfur chemisorption on W(100): Antiphase boundaries with point defects," Surf. Sci. **219**, L628-L636 (1989).